Large Interfacial Rashba Interaction Generating Strong Spin–Orbit Torques in Atomically Thin Metallic Heterostructures

Sachin Krishnia, Yanis Sassi, Fernando Ajejas, Nicolas Sebe, Nicolas Reyren, Sophie Collin, Thibaud Denneulin, András Kovács, Rafal E Dunin-Borkowski, Albert Fert, et al.

NANO LETTERS

pubs.acs.org/NanoLett

Letter

Large Interfacial Rashba Interaction Generating Strong Spin−Orbit Torques in Atomically Thin Metallic Heterostructures

Sachin Krishnia, Yanis Sassi, Fernando Ajejas, Nicolas Sebe, Nicolas Reyren, Sophie Collin, Thibaud Denneulin, András Kovács, Rafal E. Dunin-Borkowski, Albert Fert, Jean-Marie George, Vincent Cros,* and Henri Jaffrès*

Cite This: *Nano Lett.* 2023, 23, 6785−6791

Read Online

ACCESS | Metrics & More | Article Recommendations | Supporting Information

ABSTRACT: The hallmark of spintronics has been the ability of spin−orbit interactions to convert a charge current into a spin current and vice versa, mainly in the bulk of heavy metal thin films. Here, we demonstrate how a light metal interface profoundly affects both the nature of spin−orbit torques and its efficiency in terms of damping-like (H_{DL}) and field-like (H_{FL}) effective fields in ultrathin Co films. We measure unexpectedly H_{FL}/H_{DL} ratios much larger than 1 by inserting a nanometer-thin Al metallic layer in Pt|Co|Al|Pt as compared to a similar stacking, including Cu as a reference. From our modeling, these results evidence the existence of large Rashba interaction at the Co|Al interface generating a giant H_{FL}, which is not expected from a metallic interface. The occurrence of such enhanced torques from an interfacial origin is further validated by demonstrating current-induced magnetization reversal showing a significant decrease of the critical current for switching.

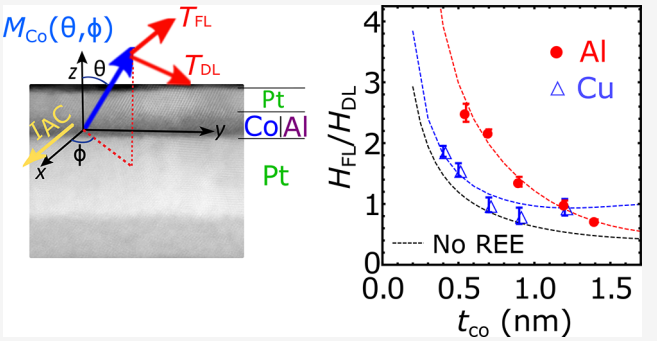

KEYWORDS: *Rashba-Edelstein effect, Spin−orbit torques, Spintronics, Magnetization switching*

In modern nanomagnetism, spin−orbit coupling (SOC) at interfaces is exploited to generate strong interfacial perpendicular anisotropy (PMA) or antisymmetric exchange interactions.[1] In spintronics, SOC is the key interaction to generate spin-current via the spin Hall effect (SHE) in heavy metals, enabling magnetization switching[2−6] and driving skyrmions[7] and domain walls. In atomically thin layers with broken inversion symmetry, the interplay of low-dimensionality and SOC may also lead to a Rashba spin-splitting[8−10] modifying the electronic ground state, thus affecting the spin transport via the Rashba−Edelstein (REE)[11] or orbital Rashba effects (ORE).[12,13] These phenomena, namely, SHE[5,14,15] and REE (or ORE),[5,10,11,15,16] may convert a charge current $\mathcal{J}_c$ into either an out-of-equilibrium spin-current $\mathcal{J}_\sigma$ or spin accumulation $\hat{\boldsymbol{\mu}}$ (out-of equilibrium spin-density) carrying an angular momentum. Upon current injection, those can, in turn, transfer their angular momentum to the adjacent ferromagnetic layer by precessing around the exchange field.

Both $\mathcal{J}_\sigma$ and $\hat{\boldsymbol{\mu}}$ may exert spin−orbit torques (SOTs) onto a magnetization vector $\mathcal{M} = M\hat{\mathbf{m}}$ with two components: damping-like torque (DLT), $\hat{\tau}_{DL} \propto \hat{\mathbf{m}} \times (\hat{\boldsymbol{\mu}} \times \hat{\mathbf{m}})$, and field-like torque (FLT), $\hat{\tau}_{FL} \propto \hat{\boldsymbol{\mu}} \times \hat{\mathbf{m}}$. The nature and strength of the corresponding DL (H_{DL}) and FL (H_{FL}) effective fields strongly depend on the relaxation of the transverse spin i.e. on the spin decoherence length, which is predicted to be a few atomic lattice parameters.[17,18] Manipulating the magnetization via SOTs and disentangling the exact origin of SOTs to use them adequately are still challenging today for writing processes in magnetoelectronic devices.

In the pioneer experiments by Miron et al. in Pt|Co|AlO_x,[2] SOT was discussed in terms of dominating FLT arising from REE at the Co|Oxide interface, larger than SHE-DLT from Pt, suggesting the crucial role of a large interfacial electric field at the ferromagnet/oxide interface. Although, in metals, SHE is largely considered as the primary source of DLT,[3,19−21] a significant interfacial REE has been recently observed in Ir|ferromagnetic|Ta contributing to DLT.[22] In the limit of atomically thin magnetic layers, additional mechanisms might also influence the strength of the SOTs: spin-filtering or charge quantum confinement,[23−27] surface states of topological insulators (TIs)[28] and 2D electron gases.[29]

Received: December 29, 2022
Revised: June 22, 2023
Published: July 31, 2023

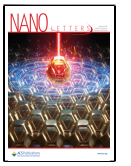

https://doi.org/10.1021/acs.nanolett.2c05091
Nano Lett. 2023, 23, 6785−6791

Moreover, recent theory has evidenced additional orbital currents in light elements from orbital Hall effects (OHE) and/or orbital Rashba effects (ORE) superimposing to the spin currents.[30] These orbital currents may result in the generation of orbital torques[12,31] and orbital Rashba magnetoresistance.[13,32] This questions the actual origin of the magnetic torques in multilayers with light elements.

In this study, we investigate the properties of SOTs in atomically thin metallic structures, namely, Co layers ranging from 1.4 nm down to 0.4 nm, sandwiched between Pt and light element overlayers, i.e., Al or Cu. Using the second harmonic Hall measurement technique,[33,34] we precisely determine the amplitude of the SOT vs the ferromagnetic film thickness, the light-element overlayer, and the heavy-element. Compared to the best-reported results,[34] we find an increase of the DLT by ∼30% together with a drastic rise in the FLT by more than ∼190%. With the help of our spin-dependent Boltzmann calculations, we explicitly demonstrate the occurrence of enhanced SOT due to a strong REE in asymmetric Pt|Co|Al| Pt stacks, from a FLT over DLT ratio as large as 2.5 for 0.55 nm thick Co, one of the highest values ever reported in metals.

Samples were grown using magnetron sputtering at the base pressure 6×10^{-8} mbar. In Figure 1a, we show X-ray

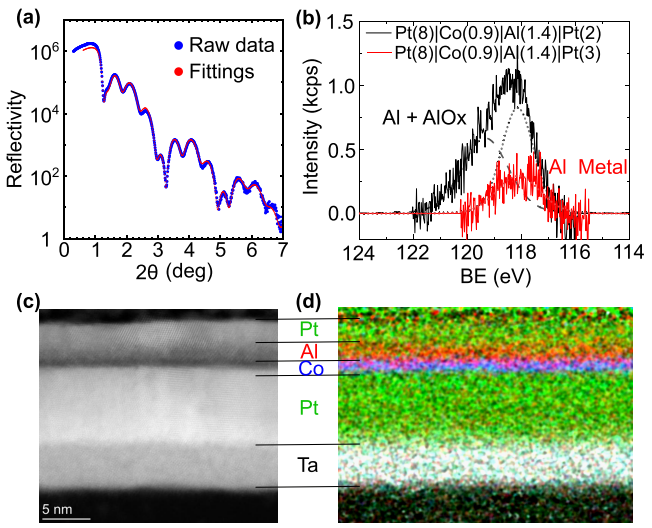

Figure 1. (a) XRR measurements (blue) and fittings (red) on Pt(8)|Co(0.7)|Al(1.4)|Pt(3) sample. (b) Measurements of XPS on similar samples are shown by red color together with a reduced Pt capping (2 nm) with oxidized Al (in black). (c) HAADF image in STEM of the sample with corresponding EDX elemental map shown in (d).

reflectivity (XRR) measurements (blue) and fit (red) on a Ta(5)|Pt(8)|Co(0.7)|Al(1.4)|Pt(3) sample where the layer thicknesses are found to be in good agreement with nominal values (<3% error). The XRR measurements reveal 0.29 and 0.12 nm roughness at Pt|Co and Co|Al interfaces, respectively, comparable with the SiO_2|Ta interface (0.45 nm). We have also performed X-ray photoelectron spectroscopy (XPS) on Pt(8)|Co(0.7)|Al(1.4)|Pt(t_{Pt}) with t_{Pt} = 2 and 3 nm to probe the chemistry of Al underneath Pt (Figure 1b with black and red colors respectively). As the Al 2*p* peak (71 eV) is totally screened by the 4*f* Pt peaks, the 2*s* Al bonds are probed. The peak for the 2 nm Pt capping can be fitted with two contributions attributed to AlOx (dashed) and metallic Al (dotted) respectively whereas the 3 nm Pt capping sample only reveals a single metallic state of Al thus discarding any oxidization state. In Figure 1c and d, we show the energy dispersive X-ray spectroscopy (EDX) measurements in scanning transmission electron microscopy (STEM). The Ta, Pt Co, and Al layers can be clearly distinguished by bright and black Z-contrasts in high-angle annular dark-field (HAADF) image. In Figure 1d, we show elemental distribution of Ta (white), Pt (green), Co (blue), and Al (red). Together with XRR, the HAADF and EDX characterizations clearly show homogeneous and flat interfaces without any sign of oxidation of the Al film.

To evaluate the two components of the SOTs, we employed the harmonic Hall measurement technique on 5 μm wide Hall bars with an AC excitation of 727 Hz (SI-I). First, we compare the results from the two series of multilayers with Al and Cu light element interfaced with Co: Pt(8)|Co(t_{Co})|Al(1.4)|Pt(3) and Pt(8)|Co(t_{Co})|Cu(1.4)|Pt(3). Starting from negligible torques in a fully symmetric Pt(8)|Co(0.9)|Pt(8) stack as expected (SI-V), the asymmetric "control" sample Pt(8)|Co(0.9)|Pt(3) gives H_{DL} = 0.80 ± 0.05 mT and H_{FL} 0.58 ± 0.15 mT for a current density $\mathcal{J}_{Pt}$ in Pt = 10^{11} A/m^2 (later used as a reference value). To obtain integrated torques over the whole ferromagnetic layer of thickness t_{Co} and hence to be able to make an accurate comparison, we define a normalized quantity by multiplying $H_{DL,FL}$ with t_{Co} for a 10^{11} A/m^2 current density in Pt. This corresponds to the equivalent torque values for an applied electric field $\mathcal{E} = \rho_{Pt} \times \mathcal{J}_{Pt} = 2.5 \times 10^4$ V/m owing to the Pt resistivity ρ_{Pt} = 25 $\mu\Omega$·cm (SI-III). Our analyses mainly depend on the anisotropy field H_k, but not on the saturation magnetization at the limit of thin Co M_s = 1.1 ± 0.1 MA/m, remaining however quite independent of the Co thickness t_{Co} for both the Al and Cu series (SI-IV).

Several features may be highlighted with similarities and differences between the Al and Cu series. First, as shown in Figure 2a, the integrated DL component $(H_{DL} \times t_{Co})/\mathcal{J}_{Pt}$ is

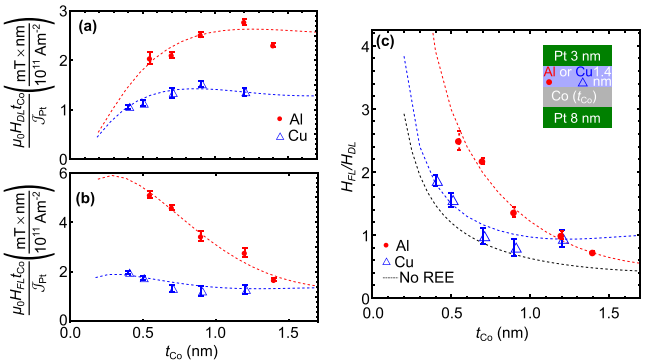

Figure 2. (a) Damping-like (DL) field and (b) field-like (FL) field multiplied by t_{Co} for $\mathcal{J}_{Pt} = 10^{11}$ A/m^2 in Pt(8)|Co(0.55−1.4)|Al(1.4)|Pt(3) and Pt(8)|Co(0.4−1.2)|Cu(1.4)|Pt(3). (c) t_{Co} dependence of $\zeta = H_{FL}/H_{DL}$. Red and blue dashed lines are fits to experimental data points using our theoretical model, and black dashed line in (c) is calculated ζ values without any Rashba interface (see SI-VII).

about 65% larger in Pt|Co|Al(1.4)|Pt samples compared to Pt|Co|Cu(1.4)|Pt for almost the whole Co thickness. At t_{Co} = 0.9 nm, the value of DLT is about 2.5 mT × nm/(10^{11} A·m^{-2}) for Al and 1.5 mT × nm/(10^{11} A·m^{-2}) for Cu. We note however that the $(H_{DL} \times t_{Co})/\mathcal{J}_{Pt}$ product exhibits in each case a similar maximum close to t_{Co} = 1.0−1.2 nm that we ascribe to the spin decoherence length at small thickness. Second, we find

https://doi.org/10.1021/acs.nanolett.2c05091
Nano Lett. 2023, 23, 6785−6791

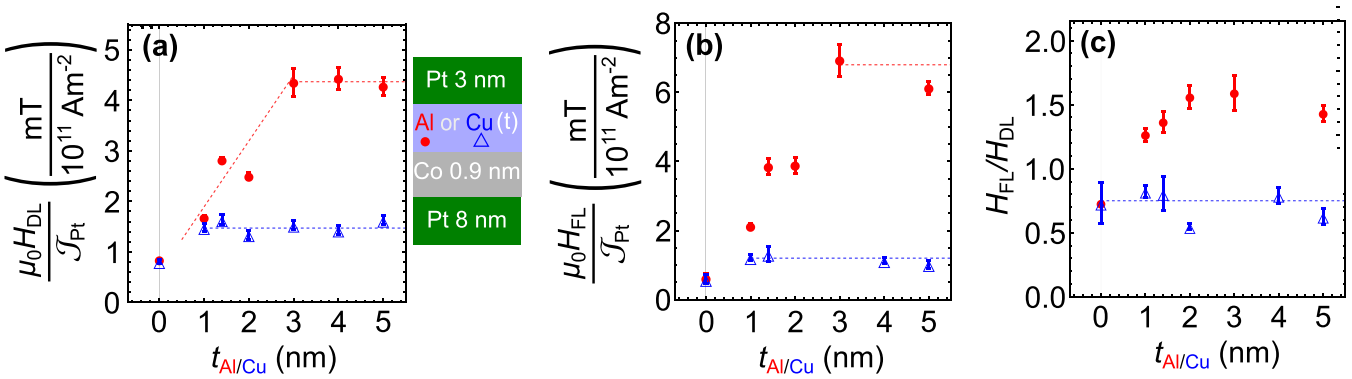

Figure 3. (a) H_{DL} vs Al (red) and Cu (blue) layer thickness. The variation in H_{DL} is fitted by the dashed red lines (SI-VII). We used l_{sf}^{Pt} = 1.5 nm, $\tilde{r}_s$ = 2, $\mathcal{L}$ = 0.4, $\theta_{SHE}^{Pt(0)}$ = 0.09 and the transmission coefficient $\mathcal{T}$ varying linearly from $\mathcal{T}$ = 0.8 for t_{Al} = 0 nm to $\mathcal{T}$ = 0 when t_{Al} > 3 nm. (b) H_{FL} vs Al (red) and Cu (blue) layer thickness. (c) $\zeta = H_{FL}/H_{DL}$ vs Al (red) and Cu (blue) layer thickness. Thick and constant blue lines are a guide to the eye.

that the FLT exhibits an increase in reducing t_{Co} (Figure 2b) in both series, resulting in a dominating FLT component at small t_{Co}. Nevertheless, their SOT magnitude strongly differs. We observe a substantial increase of the FLT for Al(1.4), i.e., from 1.7 mT × nm/(10^{11} A·m^{-2}) for t_{Co} = 1.4 nm to 5.2 mT × nm/(10^{11} A·m^{-2}) for t_{Co} = 0.55 nm, whereas the maximum value of FLT reaches only 2 mT × nm/(10^{11} A·m^{-2}) for Cu. Such a large FLT increase in the atomically thin Co layer has never been reported to our knowledge. This striking result manifests also by a rise of the FLT to DLT ratio $\zeta = \frac{H_{FL}}{H_{DL}}$ for Pt|Co|Al|Pt that we will consider as a new figure of merit (see Figure 2c).

Such a behavior is expected either for SHE when t_{Co} becomes smaller than the spin-decoherence length (black curve in Figure 2c from our modeling (SI-VII) or for an increased weight of REE (red dotted line for Al and blue for Cu in Figure 2c). We find that $\zeta = \frac{H_{FL}}{H_{DL}}$ saturates for $t_{Co} \gtrsim 1.2$ nm with a magnitude $\zeta \approx 0.7$ in the "thick" ferromagnet limit for SHE.[19] This corresponds also to the case of the Cu series with moderate Rashba effects. Similar value of $\zeta \simeq 0.7$ were also obtained on 4 nm thick Co|Ni multilayers.[35] Here, on reducing t_{Co} below 1.2 nm, ζ increases sharply for the Pt|Co|Al| Pt series (Figure 2c) and eventually reaches 2.5 for t_{Co} = 0.55 nm. This ratio remains smaller than unity down to t_{Co} = 0.7 nm for Pt|Co|Cu|Pt. Such FLT enhancement by a factor larger than three from t_{Co} = 1.4 nm to t_{Co} = 0.55 nm strongly challenges the SHE (and/or OHE) origin of SOT with Al.

In Figure 3, we present the evolution of $H_{DL}/\mathcal{J}_{Pt}$ (Figure 3a), $H_{FL}/\mathcal{J}_{Pt}$ (Figure 3b), and their ratio $\zeta = \frac{H_{FL}}{H_{DL}}$ vs Al (red points) and Cu (blue points) thickness (Figure 3c). Both DLT and FLT exhibit a strong enhancement with t_{Al} in the 1−3 nm window, particularly pronounced for the FLT. We find that FLT (respectively DLT) increases from ∼0.65 mT/10^{11} A·m^{-2} (∼0.8 mT/10^{11} A·m^{-2}) for t_{Al} = 0 nm to a saturation value of ∼7 mT/10^{11} A·m^{-2} (∼4.4 mT/10^{11} A·m^{-2}) for t_{Al} = 3 nm. This corresponds to a boost of the FLT by more than a factor of 10 upon inserting 3 nm of Al on top of 0.9 nm Co. Conversely, the ratio ζ is also enhanced with t_{Al} (Figure 3c) from ζ = 0.8 for t_{Al} = 0 to ζ = 1.6 for $t_{Al} \geq 3$ nm. First, we comment the behavior of DLT. Based on the results from our fits (SI-VII), we assign the rise of DLT vs t_{Al} to the decrease of the transmission coefficient $\mathcal{T}_{\uparrow\downarrow}^{Co/Al/Pt}$ at the top of the structure varying linearly from $\mathcal{T}_{\uparrow\downarrow}^{Co/Pt} \cong 0.8$ for t_{Al} = 0 nm to $\mathcal{T}_{\uparrow\downarrow}^{Co/Al3/Pt} \cong 0$ when t_{Al} > 3 nm. This results in the quenching of the opposite SHE from the top Pt. However, part of the DLT enhancement also originates from the conversion of the FLT into the DLT in the Co thickness via the spin precession mechanism. This trend is very different in the "reference" Cu series vs t_{Cu} as we find that $H_{DL}/\mathcal{J}_{Pt} \approx 1.5$ mT/10^{11} A·m^{-2} and $\zeta \approx 0.7$ remain roughly constant vs t_{Cu} (blue open triangles in Figure 3a and b).

Two important conclusions may then be drawn for the DLT: (i) a progressive extinction of the SHE action from the top Pt on increasing the thickness of Al through the quench of the electron transmission at the Co|Al|Pt interfaces and (ii) a larger electronic transmission across Co|Cu|Pt[36,37] partially compensating the SHE torque from the bottom Pt (irrespective of t_{Cu}). Considering both bottom and top Pt layers, the effective spin Hall angle (SHA) (θ_{SHE}^{eff}) is

$$\theta_{SHE}^{eff} \approx \theta_{SHE}^{bulkPt}[1 - \mathcal{L}][\mathcal{F}(8, \mathcal{T}_{Co|Pt}) - \mathcal{F}(3, \mathcal{T}_{Co|Al||Pt})] \quad (1)$$

where θ_{SHE}^{bulkPt} is the bare SHA of bulk Pt, $\mathcal{T}$ is the effective transmission coefficient at the top, and $\mathcal{L}$ is the spin-loss.[36,38,39] The function $\mathcal{F}$:

$$\mathcal{F}(t_{Pt}, \mathcal{T}) \approx \frac{\mathcal{T}\tilde{r}_s^{Pt}\coth\left(\frac{t_{Pt}}{\lambda_{sf}^{Pt}}\right)\left[1 - \mathrm{sech}\left(\frac{t_{Pt}}{\lambda_{sf}^{Pt}}\right)\right]}{1 + \mathcal{T}\tilde{r}_s^{Pt}\coth\left(\frac{t_{Pt}}{\lambda_{sf}^{Pt}}\right)} \quad (2)$$

describes the spin back-flow in Pt with $\lambda_{sf}^{Pt} \approx 1.5$ nm being its spin-diffusion length (SDL) in Pt as in ref 37 and $\tilde{r}_s^{Pt} \approx 2$ is its spin-resistance in the unit of the inverse of the Sharvin conductance (SI-VII). From our fitting procedure (Figure 3a), we could extract $\theta_{SHE}^{eff} = (1 - \mathcal{L})\mathcal{T}\theta_{SHE}^{bulkPt} = 0.075 \pm 0.01$ using $\theta_{SHE}^{bulkPt} \approx 0.225 \pm 0.025$ in agreement with the literature for a Pt resistivity of ρ = 25 $\mu\Omega$·cm.[37,40] Similar values of θ_{SHE}^{bulkPt} were determined from AHE.[40] We considered here $\mathcal{T}_{\uparrow\downarrow}^{Co/Pt} = 0.8$ and $\mathcal{L} \approx 0.4$. Our fitting procedure applied to AHE (SI-IV) uses the same set of parameter values as for SOTs. The SHE compensation from the top injection then approaches 75% in our 'control' Pt(8)|Co(0.9)|Pt(3) structure and 60% in the Pt(8)|Co(0.9)|Cu|Pt(3) series. This implies that the expected increase of the DLT is 25% (0.75/0.6) from

https://doi.org/10.1021/acs.nanolett.2c05091
Nano Lett. 2023, 23, 6785−6791

Pt(8)|Co(0.9)|Pt(3) to Pt(8)|Co(0.9)|Cu|Pt(3) and by a factor ×2.5 to Pt(8)|Co(0.9)|Al(3)|Pt(3) (Figure 3a).

In order to highlight any additional REE (or ORE) arising from Co|Al, we reduced the bottom Pt thickness in the Pt(t_{Pt})|Co(0.9)|Al(5) series to attenuate the SOTs originating from SHE. We first quantified this SHE contribution by extracting θ_{SHE} from H_{DL} according to $\theta_{SHE}^{eff} = \frac{2e}{\hbar}\frac{\mu_0 H_{DL} M_s t_{Co}}{\mathcal{J}_{Pt}}$ (e is the electron charge). In Figure 4a, we observe that θ_{SHE}^{eff} increases

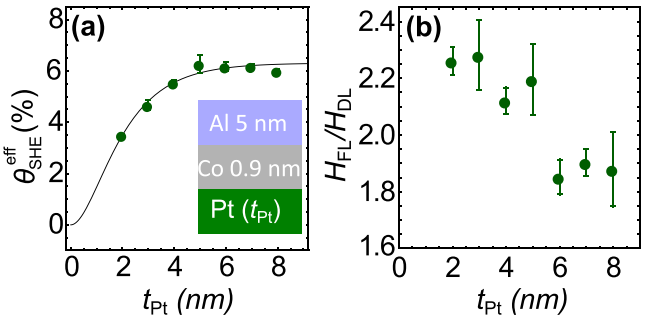

Figure 4. a) Effective θ_{SHE}^{eff} vs t_{Pt} (green points). The solid line is the fit enabling to extract l_{sf}^{Pt} = 1.5 nm, Pt bulk $\theta_{SHE}^{bulk\ Pt}$ = 0.225 ± 0.025 (effective θ_{SHE}^{eff} = 0.075 ± 0.01), and $\tilde{r}_s^{Pt}$ = 2 using eq 2. (b) Plot of the ζ ratio vs t_{Pt}.

with t_{Pt} according to $\propto \theta_{SHE}^{bulkPt} \times \mathcal{F}(t_{Pt})$ (eq 2) before reaching its saturation value for $t_{Pt} \geq 5$ nm. From the fitting procedure, the spin-diffusion length (SDL) and θ_{SHE}^{eff} are, respectively, ≃1.5 nm and ≃0.08, in agreement with data of Figure 3. In Figure 4b, we show the impact of the additional REE (or ORE) occurring from Co|Al on the SOTs for t_{Co} = 0.9 nm. First, the FLT clearly dominates the DLT for all the Pt thicknesses. In addition, a remarkable increase of ζ is observed at the lowest t_{Pt} = 2−5 nm thickness range, i.e., where SHE has not yet reached its maximum efficiency. This undoubtedly supports the role of a significant Rashba interaction (i.e., REE and/or ORE) superimposed to SHE. Our data also yield a clear quantitative understanding of how the Rashba effects at metallic interfaces may strongly affect H_{FL} in chemically asymmetric Pt|Co|Al|Pt stacks (see Figures 2 and 3).

We then performed SOT-driven magnetization switching experiments on Pt(8)|Co(0.9)|Al(t_{Al})|Pt(3) Hall cross-bars. A magnetic field H_x, either positive or negative, is applied along the current direction to break the mirror symmetry, and R_{AHE} is measured vs the current. Typical results of SOT-induced magnetization reversal are shown in Figure 5 for respective positive $\mu_0 H_x$ = +250, 373, 495, and 608 mT (Figure 5a) and equal negative $\mu_0 H_x$ = −240, −368, −495, and −600 mT (Figure 5b) fields for t_{Al} = 3 nm. A complete magnetization reversal is observed for $J_c \approx \pm 2{-}2.5 \times 10^{11}$ A·m^{-2} with the polarity of the magnetization reversal cycle depending on the sign of $\mu_0 H_x$ as expected. We also find that the critical current density decreases as $|\mu_0 H_x|$ increases as observed in refs 35 and 41 with the typical current density reaching J_c = 3−3.5 × 10^{11} A·m^{-2}. In Figure 5c, we compare magnetization reversal cycles for different t_{Al} = 1, 2, 3, and 4 nm, acquired under a field $\mu_0 H_x$ = +250 mT much smaller than the anisotropy field H_K (SI-IV). Despite a larger H_K and larger coercive field, we find that a complete switching of magnetization (between P and AP states) may be achieved in devices with t_{Al} = 3 and 4 nm, whereas the ones with t_{Al} = 1 and 2 nm exhibit only partial reversal, thus in agreement with the enhanced SOT shown in

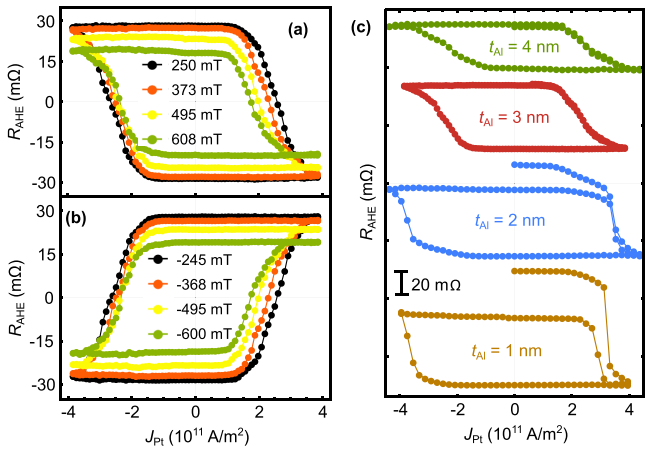

Figure 5. Current-induced magnetization reversal in Pt(8)|Co(0.9)|Al(3)|Pt(3) for different (a) positive and (b) negative $\mu_0 H_x$. (c) R_{AHE} as a function of pulsed current in the Pt(8)|Co(0.9)|Al(t_{Al})|Pt(3) series of samples for $\mu_0 H_x$ = +250 mT. The pulse width was 100 μs.

Figure 3. We hence conclude that increasing the Al thickness in the Pt(8)|Co(0.9)|Al(t_{Al})|Pt(3) series increases the SOT allowing a reduction of the critical current density for complete magnetization switching by more than 30%.

The ensemble of the results highlighting the existence of a large interfacial Rashba effect from the Co|Al is supported by our modeling (SI-VII). In the case of thick ferromagnet, it is known that SOT from SHE is determined via the complex spin-mixing conductance.[21,42,43] For t_{Co} smaller than the dephasing length, the description is far more complex owing to the remaining outgoing spin-currents and additional electronic reflections. We developed numerical analyses gathering most of the ingredients discussed above based on generalized drift-precession-diffusion equations[20,44−46] able to express the profile of the vectorial spin-accumulation $\hat{\boldsymbol{\mu}}_F$. We thus provide subsequent insights for H_{DL} and H_{FL}, the integrated value of the torque $\boldsymbol{\tau}_{SOT}$, by considering the precessing and dephasing processes via the $s-d$ exchange coupling ($\mathcal{J}_{xc}$). In particular, this implies a complex value of the propagating length in Co. The SOT acting on the Co layer by the out-of equilibrium spin $\hat{\boldsymbol{\mu}}_F$ then writes:[47]

$$\boldsymbol{\tau}_{SOT} = \int_{\mathcal{V}} \frac{d\hat{\mathcal{M}}}{dt} d\mathcal{V} \approx \int_{\mathcal{V}} \frac{\hat{\boldsymbol{\mu}}_F \times \hat{\mathbf{m}}}{\tau_J} d\mathcal{V} \quad (3)$$

where $\mathcal{V}$ is the volume of Co and μ_F is expressed in the same unit ($\mu_B/\mathcal{V}$) as $\hat{\mathcal{M}}$ and $\tau_J = \frac{\hbar}{\mathcal{J}_{xc}}$ is the precession time. In our treatment, the interfaces are described by their proper interfacial G_s or spin-mixing $G_{\uparrow\downarrow}$ (between Co and the nonmagnetic material) conductances normalized by their Sharvin values G_{sh}, or using corresponding transmission coefficients (spin-mixing transmission). It generally leads to possible spin-backflow processes[48] and additional spin-accumulation within the different layers. We considered:

(i) a typical precession (or Larmor) length $\lambda_J = 2\pi v_F \tau_J$ = 4.7 nm for the transverse part of the spin accumulation and spin-current and a transverse spin-decoherence length $\lambda_\perp$ of 1.7 nm in the range of the values given in ref 45 for Co.

(ii) a large spin-mixing transmission coefficient $\mathcal{T}_{\uparrow\downarrow}^{Co|Pt} = \frac{G_{\uparrow\downarrow}^{Co|Pt}}{G_{sh}} \approx 0.8$ at the Co|Pt interface[40,49] with $G_{\uparrow\downarrow}$ and

https://doi.org/10.1021/acs.nanolett.2c05091
Nano Lett. 2023, 23, 6785−6791

G_{sh} being, respectively, the spin-mixing conductance and the Sharvin conductance.

(iii) a mean spin-mixing transmission coefficient $\mathcal{T}_{\uparrow\downarrow}^{CoICuIPt} = \frac{G_{\uparrow\downarrow}^{CoICuIPt}}{G_{sh}} \approx 0.5 \pm 0.05$ through Cu.[36,37]

(iv) a mean spin-mixing transmission coefficient $\mathcal{T}_{\uparrow\downarrow}^{CoIAlIPt} = \frac{G_{\uparrow\downarrow}^{CoIAlIPt}}{G_{sh}}$ varying from 0.8 to 0 when the Al thickness is increased from 0 to 3 nm and greater.

Based on our present knowledge for the CoIPt interface,[36,49,50] the predicted SOT fields are in excellent agreement with the experimental ones for both DL and FL (see dashed lines in Figures 2 and 3). We accounted for a spin-accumulation $\mu_F = \mu_{REE}$ at the CoIAl(Cu) interface due to REE. For PtICoICuIPt, we consider that μ_{REE} is *homogeneous* in Co and constant for all t_{Co}. We quantify that REE (SHE) contributes ≈ 45% to the FLT (≈ 55%) for t_{Co} = 0.4 nm in the reference Cu samples. The important result is that, for the PtI CoIAlIPt series, a much larger spin accumulation μ_{REE} is required to fit the data with a certain dependence on t_{Co} varying within a length scale of the order of 0.75 nm. Consequently, the FLT contribution from REE (and/or ORE) reaches ≈75% for t_{Co} = 0.55−1.2 nm (≈ 25% from SHE), whereas it contributes only 60% for t_{Co} = 1.4 nm (≈ 40% from SHE).

Finally, we point out that, at this stage, and owing to the same symmetry of torques possibly generated by an ORE[13] compared to the one by spin Rashba effect, we cannot distinguish between the two mechanisms and thus cannot discard that a large part of the FLT increase in Al-based samples may indeed originate principally from ORE. Note, however, we can discard the role of the OHE in the Al light element (nonetheless calculated to be small[30,51]) from our results displayed in Figure 4 on the basis of the same arguments discussed for the spin Hall effect.

In conclusion, we have demonstrated that, in atomically thin Co, the SOT amplitudes, both for damping- and field-like symmetries, vary significantly when a light element such as Al is deposited on top of Co, exceeding the values existing in the literature. In particular, we find a large increase of the field-like component and the corresponding ratio of H_{FL}/H_{DL} at CoIAl IPt interfaces within the single atomic Co thickness range. This demonstrates the occurrence of interfacial Rashba interactions, leading to significant conversion effects at the CoIAl interface. Beyond the fundamental interest, these results in all-metallic systems in the limit of atomically thin ferromagnets also open a new research direction for CMOS-compatible and cost-effective spinorbitronic based technology.

■ ASSOCIATED CONTENT

Supporting Information

The Supporting Information is available free of charge at https://pubs.acs.org/doi/10.1021/acs.nanolett.2c05091.

(Detailed analysis of harmonic Hall measurements, measurements of resistivity and estimation of current shunt effects in the each layer of multilayers, theoretical modeling of anomalous Hall effect and spin−orbit torques PDF)

■ AUTHOR INFORMATION

Corresponding Authors

Vincent Cros − *Unité Mixte de Physique, CNRS, Thales, Université Paris-Saclay, 91767 Palaiseau, France;* orcid.org/0000-0003-0272-3651; Email: vincent.cros@cnrs-thales.fr

Henri Jaffrès − *Unité Mixte de Physique, CNRS, Thales, Université Paris-Saclay, 91767 Palaiseau, France;* Email: henri.jaffres@cnrs-thales.fr

Authors

Sachin Krishnia − *Unité Mixte de Physique, CNRS, Thales, Université Paris-Saclay, 91767 Palaiseau, France*

Yanis Sassi − *Unité Mixte de Physique, CNRS, Thales, Université Paris-Saclay, 91767 Palaiseau, France*

Fernando Ajejas − *Unité Mixte de Physique, CNRS, Thales, Université Paris-Saclay, 91767 Palaiseau, France;* Present Address: Department of Physics and Center for Advanced Nanoscience, University of California, San Diego La Jolla, CA, 92093, USA

Nicolas Sebe − *Unité Mixte de Physique, CNRS, Thales, Université Paris-Saclay, 91767 Palaiseau, France*

Nicolas Reyren − *Unité Mixte de Physique, CNRS, Thales, Université Paris-Saclay, 91767 Palaiseau, France;* orcid.org/0000-0002-7745-7282

Sophie Collin − *Unité Mixte de Physique, CNRS, Thales, Université Paris-Saclay, 91767 Palaiseau, France*

Thibaud Denneulin − *Ernst Ruska-Centre for Microscopy and Spectroscopy with Electrons (ER-C 1) and Peter Grünberg Institut (PGI-5), Forschungszentrum Jülich GmbH, 52425 Jülich, Germany*

András Kovács − *Ernst Ruska-Centre for Microscopy and Spectroscopy with Electrons (ER-C 1) and Peter Grünberg Institut (PGI-5), Forschungszentrum Jülich GmbH, 52425 Jülich, Germany;* orcid.org/0000-0001-8485-991X

Rafal E. Dunin-Borkowski − *Ernst Ruska-Centre for Microscopy and Spectroscopy with Electrons (ER-C 1) and Peter Grünberg Institut (PGI-5), Forschungszentrum Jülich GmbH, 52425 Jülich, Germany;* orcid.org/0000-0001-8082-0647

Albert Fert − *Unité Mixte de Physique, CNRS, Thales, Université Paris-Saclay, 91767 Palaiseau, France*

Jean-Marie George − *Unité Mixte de Physique, CNRS, Thales, Université Paris-Saclay, 91767 Palaiseau, France*

Complete contact information is available at: https://pubs.acs.org/10.1021/acs.nanolett.2c05091

Notes

The authors declare no competing financial interest.

■ ACKNOWLEDGMENTS

This work has been supported by DARPA TEE program grant (MIPRHR - 0011831554), ANR grant STORM (ANR-22-CE42-0013-02), the FLAG - ERA Sograph MEM (ANR-15-GRFL-0005) and the Horizon2020 Framework Program of the European Commission, under FETProactive Grant agreement No. 824123 (SKYTOP) (H2020 FET proactive 824123). This research was funded by the French National Research Agency under the project "ORION" ANR-20-CE30-0022-02 and as part of the "Investissements d'Avenir" program (Labex NanoSaclay, reference: SPiCY ANR-10-LABX-0035). N. Sebe benefits from a France 2030 government grant managed

https://doi.org/10.1021/acs.nanolett.2c05091
Nano Lett. 2023, 23, 6785−6791

by the French National Research Agency (ANR-22-PEPR-0009 Electronique-EMCOM).

REFERENCES

(1) Soumyanarayanan, A.; Reyren, N.; Fert, A.; Panagopoulos, C. Emergent phenomena induced by spin−orbit coupling at surfaces and interfaces. *Nature* **2016**, *539*, 509−517.

(2) Miron, I. M.; Garello, K.; Gaudin, G.; Zermatten, P.-J.; Costache, M. V.; Auffret, S.; Bandiera, S.; Rodmacq, B.; Schuhl, A.; Gambardella, P. Perpendicular switching of a single ferromagnetic layer induced by in-plane current injection. *Nature* **2011**, *476*, 189−193.

(3) Liu, L.; Lee, O. J.; Gudmundsen, T. J.; Ralph, D. C.; Buhrman, R. A. Current-induced switching of perpendicularly magnetized magnetic layers using spin torque from the spin Hall effect. *Phys. Rev. Lett.* **2012**, *109*, 096602.

(4) Razavi, A.; Wu, H.; Shao, Q.; Fang, C.; Dai, B.; Wong, K.; Han, X.; Yu, G.; Wang, K. L. Deterministic spin−orbit torque switching by a light-metal insertion. *Nano Lett.* **2020**, *20*, 3703−3709.

(5) Manchon, A.; Železný, J.; Miron, I. M.; Jungwirth, T.; Sinova, J.; Thiaville, A.; Garello, K.; Gambardella, P. Current-induced spin-orbit torques in ferromagnetic and antiferromagnetic systems. *Rev. Mod. Phys.* **2019**, *91*, 035004.

(6) Wu, H.; Nance, J.; Razavi, S. A.; Lujan, D.; Dai, B.; Liu, Y.; He, H.; Cui, B.; Wu, D.; Wong, K.; Sobotkiewich, K.; Li, X.; Carman, G. P.; Wang, K. L. Chiral symmetry breaking for deterministic switching of perpendicular magnetization by spin−orbit torque. *Nano Lett.* **2021**, *21*, 515−521.

(7) Fert, A.; Reyren, N.; Cros, V. Magnetic skyrmions: advances in physics and potential applications. *Nature Reviews Materials* **2017**, *2*, 17031.

(8) Bychkov, Y. A.; Rashba, É. I. Properties of a 2D electron gas with lifted spectral degeneracy. *Soviet Journal of Experimental and Theoretical Physics Letters* **1984**, *39*, 78.

(9) Mihai Miron, I.; Gaudin, G.; Auffret, S.; Rodmacq, B.; Schuhl, A.; Pizzini, S.; Vogel, J.; Gambardella, P. Current-driven spin torque induced by the Rashba effect in a ferromagnetic metal layer. *Nat. Mater.* **2010**, *9*, 230−234.

(10) Manchon, A.; Koo, H. C.; Nitta, J.; Frolov, S. M.; Duine, R. A. New perspectives for Rashba spin-orbit coupling. *Nat. Mater.* **2015**, *14*, 871−882.

(11) Edelstein, V. Spin polarization of conduction electrons induced by electric current in two-dimensional asymmetric electron systems. *Solid State Commun.* **1990**, *73*, 233−235.

(12) Ding, S.; Ross, A.; Go, D.; Baldrati, L.; Ren, Z.; Freimuth, F.; Becker, S.; Kammerbauer, F.; Yang, J.; Jakob, G.; Mokrousov, Y.; Kläui, M. Harnessing orbital-to-spin conversion of interfacial orbital currents for efficient spin-orbit torques. *Phys. Rev. Lett.* **2020**, *125*, 177201.

(13) Ding, S.; Liang, Z.; Go, D.; Yun, C.; Xue, M.; Liu, Z.; Becker, S.; Yang, W.; Du, H.; Wang, C.; Yang, Y.; Jakob, G.; Kläui, M.; Mokrousov, Y.; Yang, J. Observation of the orbital rashba-edelstein magnetoresistance. *Phys. Rev. Lett.* **2022**, *128*, 067201.

(14) Hirsch, J. E. Spin Hall effect. *Phys. Rev. Lett.* **1999**, *83*, 1834−1837.

(15) Sinova, J.; Valenzuela, S. O.; Wunderlich, J.; Back, C. H.; Jungwirth, T. Spin Hall effects. *Rev. Mod. Phys.* **2015**, *87*, 1213−1260.

(16) Sánchez, J. C. R.; Vila, L.; Desfonds, G.; Gambarelli, S.; Attané, J. P.; De Teresa, J. M.; Magén, C.; Fert, A. Spin-to-charge conversion using Rashba coupling at the interface between non-magnetic materials. *Nat. Commun.* **2013**, *4*, 2944.

(17) Taniguchi, T.; Yakata, S.; Imamura, H.; Ando, Y. Penetration depth of transverse spin current in ferromagnetic metals. *IEEE Trans. Magn.* **2008**, *44*, 2636−2639.

(18) Ghosh, A.; Auffret, S.; Ebels, U.; Bailey, W. E. Penetration depth of transverse spin current in ultrathin ferromagnets. *Phys. Rev. Lett.* **2012**, *109*, 127202.

(19) Stiles, M. D.; Zangwill, A. Anatomy of spin-transfer torque. *Phys. Rev. B* **2002**, *66*, 014407.

(20) Haney, P. M.; Lee, H.-W.; Lee, K.-J.; Manchon, A.; Stiles, M. D. Current induced torques and interfacial spin-orbit coupling: Semiclassical modeling. *Phys. Rev. B* **2013**, *87*, 174411.

(21) Amin, V. P.; Stiles, M. D. Spin transport at interfaces with spin-orbit coupling: Phenomenology. *Phys. Rev. B* **2016**, *94*, 104420.

(22) Dutta, S.; Bose, A.; Tulapurkar, A. A.; Buhrman, R. A.; Ralph, D. C. Interfacial and bulk spin Hall contributions to fieldlike spin-orbit torque generated by iridium. *Phys. Rev. B* **2021**, *103*, 184416.

(23) Qiu, X.; Narayanapillai, K.; Wu, Y.; Deorani, P.; Yang, D.-H.; Noh, W.-S.; Park, J.-H.; Lee, K.-J.; Lee, H.-W.; Yang, H. Spin-orbit-torque engineering via oxygen manipulation. *Nat. Nanotechnol.* **2015**, *10*, 333−338.

(24) Emori, S.; Nan, T.; Belkessam, A. M.; Wang, X.; Matyushov, A. D.; Babroski, C. J.; Gao, Y.; Lin, H.; Sun, N. X. Interfacial spin-orbit torque without bulk spin-orbit coupling. *Phys. Rev. B* **2016**, *93*, 180402.

(25) Amin, V. P.; Zemen, J.; Stiles, M. D. Interface-generated spin currents. *Phys. Rev. Lett.* **2018**, *121*, 136805.

(26) Wang, W.; Wang, T.; Amin, V. P.; Wang, Y.; Radhakrishnan, A.; Davidson, A.; Allen, S. R.; Silva, T. J.; Ohldag, H.; Balzar, D.; Zink, B. L.; Haney, P. M.; Xiao, J. Q.; Cahill, D. G.; Lorenz, V. O.; Fan, X. Anomalous spin-orbit torques in magnetic single-layer films. *Nat. Nanotechnol.* **2019**, *14*, 819−824.

(27) Han, B.; Zhang, B.; Sun, S.; Wang, B.; Guo, Y.; Cao, J. The thickness dependence of the field-like spin−orbit torque in heavy metal/CoFeB/MgO heterostructures. *J. Appl. Phys.* **2021**, *130*, 213902.

(28) DC, M.; Grassi, R.; Chen, J.-Y.; Jamali, M.; Reifsnyder Hickey, D.; Zhang, D.; Zhao, Z.; Li, H.; Quarterman, P.; Lv, Y.; Li, M.; Manchon, A.; Mkhoyan, K. A.; Low, T.; Wang, J.-P. Room-temperature high spin-orbit torque due to quantum confinement in sputtered Bi_xSe_{1-x}) films. *Nat. Mater.* **2018**, *17*, 800−807.

(29) Noël, P.; Trier, F.; Vicente Arche, L. M.; Bréhin, J.; Vaz, D. C.; Garcia, V.; Fusil, S.; Barthélémy, A.; Vila, L.; Bibes, M.; Attané, J.-P. Non-volatile electric control of spin-charge conversion in a $SrTiO_3$ Rashba system. *Nature* **2020**, *580*, 483−486.

(30) Jo, D.; Go, D.; Lee, H.-W. Gigantic intrinsic orbital Hall effects in weakly spin-orbit coupled metals. *Phys. Rev. B* **2018**, *98*, 214405.

(31) Kim, J.; Go, D.; Tsai, H.; Jo, D.; Kondou, K.; Lee, H.-W.; Otani, Y. Nontrivial torque generation by orbital angular momentum injection in ferromagnetic-metal/Cu/Al_2O_3 trilayers. *Phys. Rev. B* **2021**, *103*, L020407.

(32) Ding, S.; Noël, P.; Krishnaswamy, G. K.; Gambardella, P. Unidirectional orbital magnetoresistance in light-metal-ferromagnet bilayers. *Phys. Rev. Res.* **2022**, *4*, L032041.

(33) Krishnia, S.; Haltz, E.; Berges, L.; Aballe, L.; Foerster, M.; Bocher, L.; Weil, R.; Thiaville, A.; Sampaio, J. a.; Mougin, A. Spin-orbit coupling in single-layer ferrimagnets: Direct observation of spin-orbit torques and chiral spin textures. *Phys. Rev. Applied* **2021**, *16*, 024040.

(34) Garello, K.; Miron, I. M.; Avci, C. O.; Freimuth, F.; Mokrousov, Y.; Blügel, S.; Auffret, S.; Boulle, O.; Gaudin, G.; Gambardella, P. Symmetry and magnitude of spin−orbit torques in ferromagnetic heterostructures. *Nat. Nanotechnol.* **2013**, *8*, 587−593.

(35) Figueiredo-Prestes, N.; Krishnia, S.; Collin, S.; Roussigné, Y.; Belmeguenai, M.; Chérif, S. M.; Zarpellon, J.; Mosca, D. H.; Jaffrès, H.; Vila, L.; Reyren, N.; George, J.-M. Magnetization switching and deterministic nucleation in Co/Ni multilayered disks induced by spin−orbit torques. *Appl. Phys. Lett.* **2021**, *119*, 032410.

(36) Rojas-Sánchez, J.-C.; Reyren, N.; Laczkowski, P.; Savero, W.; Attané, J.-P.; Deranlot, C.; Jamet, M.; George, J.-M.; Vila, L.; Jaffrès, H. Spin pumping and inverse spin Hall effect in platinum: The essential role of spin-memory loss at metallic interfaces. *Phys. Rev. Lett.* **2014**, *112*, 106602.

(37) Zhang, W.; Han, W.; Jiang, X.; Yang, S.-H.; Parkin, S. S. P. Role of transparency of platinum-ferromagnet interfaces in determining the intrinsic magnitude of the spin Hall effect. *Nat. Phys.* **2015**, *11*, 496−502.

https://doi.org/10.1021/acs.nanolett.2c05091
Nano Lett. 2023, 23, 6785−6791

(38) Berger, A. J.; Edwards, E. R. J.; Nembach, H. T.; Karis, O.; Weiler, M.; Silva, T. J. Determination of the spin Hall effect and the spin diffusion length of Pt from self-consistent fitting of damping enhancement and inverse spin-orbit torque measurements. *Phys. Rev. B* **2018**, *98*, 024402.
(39) Zhu, L.; Ralph, D. C.; Buhrman, R. A. Spin-orbit torques in heavy-metal-ferromagnet bilayers with varying strengths of interfacial spin-orbit coupling. *Phys. Rev. Lett.* **2019**, *122*, 077201.
(40) Dang, T. H.; Barbedienne, Q.; To, D. Q.; Rongione, E.; Reyren, N.; Godel, F.; Collin, S.; George, J. M.; Jaffrès, H. Anomalous Hall effect in 3*d*/5*d* multilayers mediated by interface scattering and nonlocal spin conductivity. *Phys. Rev. B* **2020**, *102*, 144405.
(41) Rojas-Sánchez, J.-C.; Laczkowski, P.; Sampaio, J.; Collin, S.; Bouzehouane, K.; Reyren, N.; Jaffrès, H.; Mougin, A.; George, J.-M. Perpendicular magnetization reversal in Pt/$[Co/Ni]_3$/Al multilayers via the spin Hall effect of Pt. *Appl. Phys. Lett.* **2016**, *108*, 082406.
(42) Brataas, A.; Bauer, G. E.; Kelly, P. J. Non-collinear magnetoelectronics. *Phys. Rep.* **2006**, *427*, 157−255.
(43) Cosset-Chéneau, M.; Vila, L.; Zahnd, G.; Gusakova, D.; Pham, V. T.; Grèzes, C.; Waintal, X.; Marty, A.; Jaffrès, H.; Attané, J.-P. Measurement of the spin absorption anisotropy in lateral spin valves. *Phys. Rev. Lett.* **2021**, *126*, 027201.
(44) Zhang, S.; Levy, P. M.; Fert, A. Mechanisms of spin-polarized current-driven magnetization switching. *Phys. Rev. Lett.* **2002**, *88*, 236601.
(45) Petitjean, C.; Luc, D.; Waintal, X. Unified drift-diffusion theory for transverse spin currents in spin valves, domain walls, and other textured magnets. *Phys. Rev. Lett.* **2012**, *109*, 117204.
(46) Kim, K.-W. Spin transparency for the interface of an ultrathin magnet within the spin dephasing length. *Phys. Rev. B* **2019**, *99*, 224415.
(47) Nikolić, B. K.; Dolui, K.; Petrović, M. D.; Plecháč, P.; Markussen, T.; Stokbro, K. First-principles quantum transport modeling of spin-transfer and spin-orbit torques in magnetic multilayers. In *Handbook of Materials Modeling: Applications: Current and Emerging Materials*; Andreoni, W., Yip, S., Eds.; Springer International Publishing: Cham, 2018; pp 1−35.
(48) Han, B.; Zhang, B.; Sun, S.; Wang, B.; Guo, Y.; Cao, J. The thickness dependence of the field-like spin−orbit torque in heavy metal/CoFeB/MgO heterostructures. *J. Appl. Phys.* **2021**, *130*, 213902.
(49) Dang, T. H. J.; Hawecker, E.; Rongione, G.; Baez Flores, D. Q.; Rojas-Sanchez, J. C.; Nong, H.; Mangeney, J.; Tignon, J.; Godel, F.; Collin, S.; Seneor, P.; Bibes, M.; Fert, A.; Anane, M.; George, J.-M.; Vila, L.; Cosset-Cheneau, M.; Dolfi, D.; Lebrun, R.; Bortolotti, P.; Belashchenko, K.; Dhillon, S.; Jaffrès, H. Ultrafast spin-currents and charge conversion at 3d-5d interfaces probed by time-domain terahertz spectroscopy. *Applied Physics Reviews* **2020**, *7*, 041409.
(50) Hawecker, J.; Dang, T.-H.; Rongione, E.; Boust, J.; Collin, S.; George, J.-M.; Drouhin, H.-J.; Laplace, Y.; Grasset, R.; Dong, J.; Mangeney, J.; Tignon, J.; Jaffrès, H.; Perfetti, L.; Dhillon, S. Spin injection efficiency at metallic interfaces probed by THz emission spectroscopy. *Advanced Optical Materials* **2021**, *9*, 2100412.
(51) Salemi, L.; Oppeneer, P. M. First-principles theory of intrinsic spin and orbital Hall and Nernst effects in metallic monoatomic crystals. *Phys. Rev. Mater.* **2022**, *6*, 095001.

https://doi.org/10.1021/acs.nanolett.2c05091
Nano Lett. 2023, 23, 6785−6791